Iranian Journal of Basic Medical Sciences

ijbms.mums.ac.ir

Pharmacological investigation of oxadiazole derivatives in Alzheimer's disease: Modulation of oxidative stress, neuroinflammation, and iNOS signaling

Amber Mahmood Minhas [1], Arif-ullah Khan [1]*, Neelum Gul Qazi [2], Humaira Nadeem [1], Fawad Ali [3]

[1] Riphah Institute of Pharmaceutical Sciences, Riphah International University, Islamabad, Pakistan
[2] Department of Pharmacy, Iqra University, Islamabad, Pakistan
[3] Department of Pharmacy, Kohat University of Science and Technology, Kohat, Pakistan

ARTICLE INFO

Article type:
Original

Article history:
Received: Jun 26, 2025
Accepted: Nov 19, 2025

Keywords:
Alzheimer's disease
Cognitive impairment
Cytokines
iNOS
Neuroprotection
Oxadiazole
Oxidative stress

ABSTRACT

Objective(s): Alzheimer's disease (AD) is a progressive neurodegenerative disorder characterized by deposition of amyloid-beta (Aβ) aggregates. Aβ peptides alter synaptic function and produce neuroinflammation. The neurotoxic mechanisms are also related to increases in the expression of iNOS (inducible nitric oxide synthase), resulting in further neuronal degeneration and memory impairment.

Materials and Methods: In the current study, we assessed the *in vivo* effect of the 1,3,4-oxadiazole derivative 2-{[5-(2-aminophenyl)-1,3,4-oxadiazol-2-yl] sulfanyl}-N-(1,3-benzothiazol-2-yl) acetamide (MA) on spatial memory and inflammatory responses induced by $AlCl_3$ administration in animals.

Results: A notable improvement in memory function was observed in the $AlCl_3$-induced group at 29th post-injection, following MA treatment (5, 10, and 20 mg/kg), as indicated by the behavioral analysis. This effect is correlated with decreases in inflammatory markers such as NFKB, IL-6/ß1, IFN-γ, TNF-α, and NO levels, as well as a reduction in expression of neurodegenerative markers: β-amyloid and p-tau (*P<0.05, **P<0.01, ***P<0.001 vs disease control). The results from our study suggested that MA significantly enhances the levels of glutathione, catalase, and glutathione S-transferase while decreasing the lipid peroxidation (LPO) in comparison to the disease control group, and also improves mitochondrial dysfunction. The effects are further enhanced when MA was used in combination with aminoguanidine (AG), an iNOS inhibitor. Molecular dynamics (MD) simulations, along with protein mRNA expression and iNOS western blotting, further supported the results of *in vivo* experiments.

Conclusion: Our study proposed that MA attenuated the cytokine release, decreased oxidative stress, and iNOS expression, leading to a decrease in neurodegeneration.

▶ Please cite this article as:
Minhas AM, Khan A, Gul Qazi N, Nadeem H, Ali F. Pharmacological investigation of oxadiazole derivatives in Alzheimer's disease: Modulation of oxidative stress, neuroinflammation, and iNOS signaling. Iran J Basic Med Sci 2026; 29: 423-437. doi: https://dx.doi.org/10.22038/ijbms.2026.89093.19230

Introduction

Alzheimer's disease (AD) is clinically manifested by gradual alteration in cognitive functioning (1) and neurologically by the formation of neurofibrillary tangles and amyloid plaques. Among the risk factors implicated in the pathophysiology of AD, aging is considered the most significant (2). Oxidative stress is also a prominent feature of AD. Previous studies have documented the role of oxidative damage to lipids, DNA, RNA, and proteins in AD and in patients with mild cognitive impairment, indicating that it is an early event in disease progression (3). Primarily, a similar pattern of oxidative damage has been observed in transgenic animal models of AD, in which increased lipid and protein oxidation contributes to amyloid plaque formation. In human cases, oxidative stress develops early, preceding both amyloid plaque accumulation and neurofibrillary tangle formation (4).

The production and accumulation of ROS (reactive oxygen species) and RNS (reactive nitrogen species) are deleterious to cells, contributing to cellular injury and stimulating apoptosis (5). RNS are produced during the synthesis of nitric oxide (NO), especially when free radicals like superoxide (O2-) react with NO. NO is synthesized by nitric oxide synthase (NOS), which has three isoforms, namely endothelial (eNOS), neuronal (nNOS), and inducible (iNOS) (6). The over-reactivity of NOS, especially inducible nitric oxide synthase (iNOS), during the process of neuroinflammation, leads to elevated levels of NO (7). The neuronal damage caused by NO contributes to different neurodegenerative disorders such as AD, Amyotrophic Lateral Sclerosis, and Parkinson's disease (8).

***Corresponding author:** Arif-ullah Khan. Dean and Director, Riphah Institute of Pharmaceutical Sciences, Riphah International University, Islamabad, Pakistan. Email: arif.ullah@riphah.edu.pk

Mitochondrial dysfunction is a characteristic feature of AD, leading to oxidative stress and decreased neural energy. The alteration in the electron transport chain complexes (ETC), significantly NADH dehydrogenase (Complex I) and cytochrome C oxidase (Complex IV), causes an increase in ROS and dysregulates ATP (adenosine triphosphate) levels.

Intraperitoneal (ip)administration of aluminum chloride ($AlCl_3$) results in neuronal degeneration and memory alteration (9). Previous studies have reported that $AlCl_3$ administration increases iNOS expression in the animal brain, thereby promoting an inflammatory response. NOS inhibitors, such as aminoguanidine (AG), could alleviate the neurotoxic effects induced by $AlCl_3$, highlighting the role of iNOS in neuronal alterations—specifically, the up-regulation of iNOS exacerbates AD and dementia (10). Therefore, the current investigation focuses on the potential of iNOS inhibitors as a novel therapeutic approach for AD treatment. iNOS is responsible for accelerated neuronal death and the production of pro-inflammatory cytokines, such as interleukin-6 (IL-6), interleukin-1β (IL-1β), and tumor necrosis factor-α (TNF-α), which play crucial roles in neurotoxicity and spatial memory damage (11). Moreover, impairment of transforming growth factor ($TGF\text{-}\beta_1$) signaling in AD is known to promote Aβ accumulation and *tau* tangles formation. Based on this evidence, it can be suggested that blockade of iNOS may prevent the inflammatory response and nitrosative stress. Consequently, this might stop neurodegeneration and cognitive decline over time (12). Conjugated Oxadiazole compounds with benzothiazole have gained significant importance in medicinal chemistry owing to their diverse pharmacological actions. These bioactive scaffolds merge the structural diversity of oxadiazole and benzothiazole nuclei, which are independently known for their medicinal effects. A benzothiazole and its derivatives possess anti-cancer, anti-microbial, anti-proliferative, antiviral, anti-Alzheimer, anti-inflammatory, analgesic, anti-convulsant, anti-diabetic, anti-malarial, anti-histaminic, and anti-depressant activities (13). The current therapy for AD management includes drugs such as donepezil, rivastigmine, and galantamine (cholinesterase inhibitors) and Memantine (a partial NMDA receptor antagonist) with limited therapeutic potential (14). Based on the aforementioned aspects, this study aims to evaluate the pharmacological effectiveness of newly synthesized 2-{[5-(2-aminophenyl)-1,3,4-oxadiazol-2-yl] sulfanyl}-N-(1,3-benzothiazol-2-yl) acetamide (MA) (Figure 1), with prime focus on its neuroprotective, anti-oxidant, nitrosative stress, and anti-neuroinflammatory potential in an animal model of neurodegeneration.

Materials and Methods

Animals

Albino mice weighing between 25 and 30 g were housed in polypropylene boxes (n=5-6 per cage). Animals were maintained under standard environmental conditions (25 ± 2 °C and a 12 hr light:12 hr dark cycle). The animals have free access to water and food. All the experiments were performed in accordance with the guidance provided for the care and use of Laboratory Animals and ARRIVE guidelines, with prior approval by the ethics committee at the Faculty of Pharmaceutical Sciences (Ref. no. REC/RIPS/2022/15).

Chemicals and reagents

$AlCl_3$ and aminoguanidine (AG) were purchased from Sigma-Aldrich (USA). Other solvents and reagents, such as Griess reagent, 5, 5′-dithiobis (2-nitrobenzoic acid) (DTNB), trichloroacetic acid, and N-(1-naphthyl) ethylenediamine dihydrochloride, were supplied by Abcam. Formaldehyde, reduced glutathione (GSH), hydrogen peroxide (H_2O_2), and 1-chloro-2,4-dinitrobenzene (CDNP) were procured from Sigma Aldrich.

In silico analysis

The 3D structure of MA was built using ChemDraw 12 and converted to MOL2 format using Discovery Studio. After that, MA was amended using the Chimera 1.17.3 package and saved as .PDB file format (15). The Protein Data Bank and UniProt databases were utilized to obtain protein structures in PDB format. The proteins used in the current study are iNOS (PDB ID: 3NQS), nNOS (PDB ID:

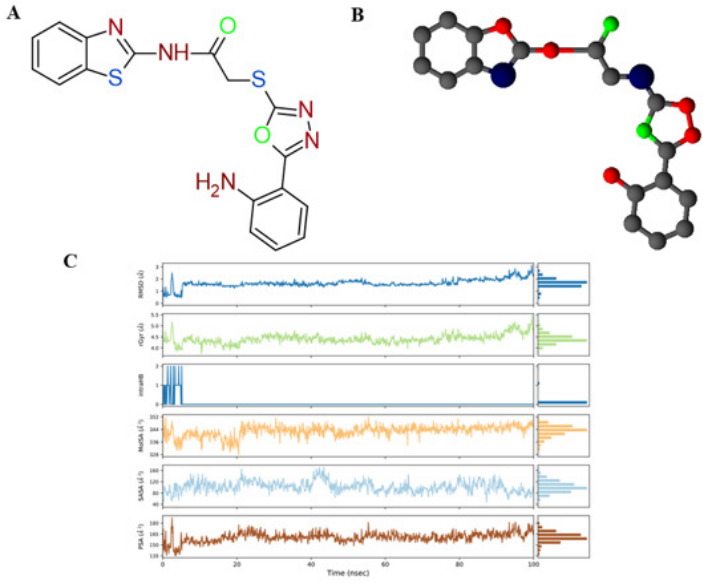

Figure 1. Ligand (2-{[5-(2-aminophenyl)-1,3,4-oxadiazol-2-yl] sulfanyl}-N-(1,3-benzothiazol-2-yl)acetamide (MA) information representation
2D and 3D structures of ligand are shown in (A) and (B) respectively, while the MA molecular surface area, radius of gyrus, intramolecular hydrogen bonds, solvent accessible surface area, and polar surface area are all represented in (C).

5VV0), and eNOS (PDB ID: 3NOS). Chimaera software tool (version 1.17.3) was used to process the crystal target protein structure for further use in *in silico* analysis. This process optimizes the unessential molecules, such as water, lipids, and unnecessary heteroatoms, from the protein sequence. The Chimera software was used to minimize energy and optimize the geometry of the macromolecular target, and the results were saved in a PDB file (16, 17). Molecular docking was carried out by employing PyRx software to express the ligand binding affinity at the active sites of the target protein. The prepared ligand and macromolecules were then added to the PyRx (18). The compound-target interactions and the macromolecule's active site were analyzed using Discovery Studio Visualizer (client 2021) software (19). The estimated parameters include amino acid residues, bond types, the number of hydrogen bonds, and other interactions between the ligand and the target protein.

Molecular dynamics simulation (MDs)

The stability of the ligand (MA) with protein (iNOS) was investigated by applying 100 ns MDs (20). The ligand-protein complex was examined by using the Schrödinger 2023-Desmond module (21), utilizing the OPLS4 force field in a precise solvent system (22). The methodology by Joung and Cheatham III (2008) was incorporated, in which the complex system was explicable in TIP3P water molecules, incorporating an orthorhombic periodic boundary box, within a 10 Å buffer zone. The unnecessary water molecules were removed, and the addition of chloride ions (Cl^-) as counterions was done in order to electrically neutralize the system. The resulting system encompasses different atoms (39,558), along with water molecules (11,590). MD simulations were performed at a constant temperature of 300 K and a pressure of 1 bar. The temperature and pressure were controlled using the Nose-Hoover thermostat and barostat (23). A hybrid energy minimization was performed over 1000 iterations, employing the steepest descent and conjugate gradient algorithms. Long-span electrostatic interactions were enumerated using the Smooth Particle Mesh Ewald (SPME) procedure to evaluate long-term electrostatic interactions. Short-span van der Waals and Coulomb's interactions were evaluated with a cut-off of 9 Å radius. A Multiple Time Step (MTS) technique, namely the Reference System Propagator Algorithm (RESPA), was used to integrate the time steps for bonded, near-bonded, and far-bonded interactions to 2, 2, and 6 femtoseconds, respectively. Simulation data were saved every 100 picoseconds, and the resulting trajectories were interpreted using the Maestro graphical interface. Principal Component Analysis (PCA) was performed using the Bio3D package (24). PCA was evaluated by using the script in the R language (25).

Research design

Aluminium chloride ($AlCl_3$) was used to induce Alzheimer 's-like disease state in mice. The animals were randomly assigned to groups of six. Mice were induced with $AlCl_3$ (40 mg/kg) daily up to 29 days. Group I was saline control and receive normal saline 10 ml/kg, Group II was disease control and receive $AlCl_3$ (40 mg/kg) IP up to 29 days, group III-V (treatment group): received protective doses of MA (5, 10 and 20 mg/kg) respectively, precisely 0.5 hr before $AlCl_3$ administration; group VI received (MA 30 mg/kg+ AG 100 mg/kg + $AlCl_3$ 40 mg/kg), mice were treated with inhibitor before $AlCl_3$ administration; group VII (positive control group), mice were treated with standard drug donepezil (5 mg/kg) (26). On the 30th day, mice underwent behavioral evaluation to assess learning and memory status. Following behavioral analysis, animals were euthanized, and brain tissue was collected for subsequent molecular analysis (Figure 2).

Behavioral paradigm

Morris water maze (MWM) test

To assess cognitive decline associated with $AlCl_3$ and the animal's spatial learning ability, the MWM test was performed according to the established protocol, with minor modifications. A circular pool was used to test learning and memory in animals. A hidden platform (10 cm) was placed approximately 1 cm below the water level, and its position was kept fixed throughout the experiment. The apparatus was hypothetically divided into four quadrants, and animals were released from different quadrants during the trial sessions. The animals underwent four trials. The latency interval (seconds) for mice in each training session, path length (m), time spent in different quadrants, and percent time spent in the target quadrant in the probe test were determined (27). The position of the platform was kept the same throughout the experiment. The platform was removed on day 5 during the probe trial. Latency (s), time spent in the target quadrant, and path length (m) were determined using the ANY-maze software.

Elevated plus maze (EPM)

This apparatus consists of four arms with a plus-shaped structure (two closed and two open), each elevated 40 cm above ground level. Animals were individually placed at the center and allowed to explore the apparatus, with particular attention to their heads facing the open arm. The parameters noted include the number of entries into the open arms and the time spent in the open arms (28).

Open field test (OFT)

This test was conducted to assess exploratory behavior and locomotion according to a previously established protocol, with minor modifications. Behavioral assessments, including time spent by mice in the central square, the number of rears, and time to leave the central zone, were recorded. The entry or exit towards the one zone was considered only when the mice were retained with all four feet in one square (29).

Y-maze test

A Y-shaped apparatus was used to analyze animal behavior. It consisted of three arms (A, B, and C) with specifications of each arm as ≈20 cm height, 10 cm width, and 40 cm length. The animals were placed at the center of the apparatus and allowed to explore the arms for 8 mins (27). The number of entries and percent alternations were calculated as follows: % alternation=number of alternations/total number of entries-2 X 100. The increase in % alternation behavior (%) represents the restoration of memory functioning.

Experimental protocol for multiple time-point behavioral evaluation of MA at different doses

To evaluate the time and dose-dependent effect of the test compound, baseline trial analysis was conducted for each group (I-VII) prior to the initiation of dosing.

Following the initial baseline observation, animals were subjected to behavioral assessment at multiple points, i.e., day 3rd, 7th, 11th, 15th, 19th, 23rd, 27th, and 29th. The parameters observed in each trial were learning and cognitive behavior with different doses of MA (5, 10, and 20 mg/kg). After the completion of each trial, the animals were placed in specific cages. In order to minimize the stress and to ensure consistency, animals were subjected to single training sessions per day (30).

Brain tissue collection for biochemical analysis

Following completion of behavioral analysis, the animals underwent biochemical evaluation, including the estimation of neuroinflammatory markers. Following euthanasia, the brain tissues of the animals were extracted onto an ice-cold glass plate. The brain tissues were stored at -80 °C for biochemical analysis. The brain tissues were then centrifuged at 2000-3000 rpm for~15 min. The homogenate was separated and utilized for further analysis at 4 °C (31).

Oxidative stress markers

Tissue anti-oxidant assay for glutathione (GSH), catalase, glutathione-S-transferase, and lipid peroxidase (LPO) was performed for the neuroprotective role of MA against $AlCl_3$-induced oxidative stress (32). For the GSH assay, supernatant (0.2 ml) was added to the DTNB (0.2 ml), and the final volume was made up to 3 mL with phosphate buffer (0.2 M). The absorbance was measured at 412 nm using a spectrophotometer and expressed as µmol/mg of protein. The GST activity was evaluated by adding CDNB (1 mM) and GSH (5 mM) to a 0.1 M phosphate buffer. Approximately 60 µl of the tissue homogenate was added to the mixture, and the absorbance was measured at 340 nm using an ELISA plate reader. Catalase activity was measured in phosphate buffer (pH 7.4), and absorbance was recorded at 312 nm. The enzymatic activity was expressed as units per milligram of protein (U/mg protein). Lipid peroxidation (LPO) levels were determined by thiobarbituric acid reactive substances (TBARS). For this test, homogenate solution (200 µl) was reacted with 0.1 M phosphate buffer (580 µl, pH 7.4), followed by the addition of 100 mM ascorbic acid (200 µl) and ferric chloride (20 µl). The reaction mixture was incubated at 37 °C for 1 hr in a water bath. 10% trichloroacetic acid (TCA) and 1000 µl of 0.66% thiobarbituric acid (TBA) were added to terminate the reaction, and the absorbance of the resulting supernatant was measured at 535 nm against a blank. Results were expressed as TBARS (nmol per mg of protein).

Indicators of biological inflammation

The estimation of cytokines, including IL-6(PRS20303 M0), IL-1ß (PRS-20295Mo), IFN-γ (MBS25001o5), NFKB(E-El-R0676), TNF-α (E-El-R0019), and TGF-β1 (ab119557), was estimated using an ELISA kit according to the manufacturer's protocol and expressed as pg/ml or ng/l (33). AD-specific markers β-amyloid (PRS-20038 Mo) and p-*tau* (PRS-31054) were also estimated according to the established protocol.

Assessment of mitochondrial functioning markers

Mitochondrial function was assessed by measuring the levels of complex I, complex IV, and ATP in the brain tissues of the tested animals (n=6) using a standard protocol. The results were quantified spectrophotometrically (34).

Nitric oxide (NO) assay

To evaluate NO levels, nitrite concentration in mouse brain tissue was measured using the Griess reagent. The testing mixture was devised, consisting of saline (50 µl), Griess reagent (50 µl), and supernatant of the homogenized tissue (50 µl). The resultant solution was then incubated at 37 °C for 0.5 hr. The absorbance was evaluated at 540 nm using a microplate reader. Sodium Nitrite mixture was used as a standard to realign the absorbance coefficient (35).

Cresyl violet-nissl staining

To perform brain tissue staining, de-paraffinization was performed by using two portions of xylene. Subsequently, slide rehydration was performed using ethanol at different concentrations (absolute, 70, 50, and 30%) for 5 min in each step and finally rinsed with distilled water for 2 min. The slides were then merged in sodium thiosulfate solution (10%) for 60 sec, washed, and placed in distilled water for 5 min. The slides were then incubated with cresyl violet (1%) solution in buffer for approximately 20 min at 60 °C. At the end, the slides were rehydrated with ethanol in ascending concentration, i.e., 30, 50, 70 %, and absolute. Images were acquired using an Olympus light microscope (Japan) at 40X and analyzed using ImageJ software (36).

iNOS gene expression

The messenger RNA (mRNA) expression levels were measured using Real Time Polymerase Chain Reaction RT-PCR analysis (37). The TRIZOL method was utilized for the extraction of total ribonucleic acid (RNA) from the homogenized brain tissue, according to the manufacturer's instructions. The complementary DNA (cDNA) was prepared from 1-2 µg of RNA content using reverse transcriptase enzyme. cDNA was then amplified by employing an RT-PCR thermocycler. The gene expression of mRNA was then normalized to the housekeeping gene (GAPDH). Relative changes in mRNA gene expression were calculated using the 2^-ΔΔCt method, also known as comparative cycle threshold (C_T). Primer sequences used for iNOS genes were CAGAAGCAGAATGTGACCATC (Forward): CAGAAGCAGAATGTGACCATC (Reverse), and for GAPDH, CAACTCCCTCAAGATTGTCAGCAA (Forward): GGCATGGACTGTGGTCATGA (Reverse).

iNOS expression by Western blot analysis

iNOS levels were measured by western blot analysis to determine the role of iNOS in $AlCl_3$-induced AD-like disease. The protein samples were prepared in triplicate using Laemmli buffer, vortexed, and incubated for 10 min at 96 °C. Subsequently, the samples were cooled for 10 min and then vortexed again to ensure complete denaturation. The proteins were separated using SDS-PAGE (SDS polyacrylamide gel electrophoresis) based on molecular weight. The separated proteins were transferred to a PVDF (polyvinylidene fluoride) membrane for immunoblotting. The membranes were washed and fixed with skimmed milk (5%) in TBST (Tris- Buffered Saline with Tween 20) buffer to prevent non-specificity. The blocked membranes were incubated with primary antibody against iNOS (Santa

Table 1. Molecular docking analysis showing atomic contact energies (kcal/mol), no of hydrogen bonds, π-π bonds, and binding residues formed by MA and aminoguanidine (AG) with target: Inducible nitric oxide synthase (iNOS), neuronal nitric oxide synthase (nNOS), and endothelial nitric oxide synthase (eNOS)

Ligand	Target protein	E-value (kcal/mol)	H- Bonds	Binding residues	π-π Bonds	Binding residues
MA	iNOS (3NQS)	-9.9	1	CYS-200	5	PHP-369, TRP-194, (π-π stacked) ARG-199, ALA-197, LEU-209 (π-alkyl)
	nNOS	-8.4	1	HIS-697	2	TRP-683 (π-π stacked) ARG-608 (π-π alkyl)
	eNOS	-8.8	4	HAR-1012, HEM-1010, 1011, ARG-372	2	VAL-336, VAL-104 (π-π alkyl)
Amino-guanidine (AG)	iNOS (3NQS)	-4.3	3	GLY-270, ARG-159, SER-160	-	-

MA: 2-{[5-(2-aminophenyl)-1,3,4-oxadiazol-2-yl] sulfanyl}-N-(1,3-benzothiazol-2-yl)acetamide

Cruz Biotechnology, Dallas, USA) at 4 ºC overnight. After washing with TBST buffer, membranes were incubated at 25 ºC for 3 to 4 hr by using an HRP-conjugated antibody. The protein bands were visualized, quantified, and then normalized to the loading control, β-actin(38)

Statistical analysis

GraphPad Prism version 8 was used to analyze the experimental data from the tests. The final results were expressed as mean along with the standard error of the mean (SEM). Two-way ANOVA followed by *post hoc* Tukey's test was applied for analysis. Results were considered different at a significance level of $P<0.05$.

Results

Molecular docking and visualization

The docking analysis provides an assessment of binding energies and the number of hydrogen bonds formed between the ligand and the protein complex. The *in silico* analysis demonstrated that MA exhibited a higher binding affinity for iNOS than other isoforms. Table 1 presents the binding energy values, hydrogen-bonding interactions, and other interactions of MA with NOS isoforms. The iNOS pathway was prioritized for further detailed analysis because MA exhibited the strongest binding interaction (highest binding energy) with iNOS among the targets. The 2D interaction of ligands with the targets is shown in Figure 2.

Ligand information

The detailed information on the ligand (MA) was shown in Figure 1-C, including polar surface area (PSA) contributed by oxygen and nitrogen atoms, solvent accessible surface area (SASA) accessible by water molecules, Molecular surface area (MolSA) with 1.4 Å probe radius showing it to be equivalent to vander waals surface area, intramolecular hydrogen bonds (intraHB) within a ligand, radius of gyration (rGyr) showing ligand extendedness, and root mean square deviation (RMSD).

Target protein information

The simulation studies were executed to obtain the information relevant to protein, including the total number of residues, protein chains, and the number of atoms- heavy as well as charged atoms in the target (3NQS), as shown in Figure 3-A. Part B shows the RMSF; low RMSF values at most sites suggest stiffness, particularly for protein core or binding-site residues. The RMSF is stable in interacting residues and flexible in key regions. Optimization and drug design use interaction analysis to find ligand-binding residues. Ligand-interacting green residues are stable due to binding constraints. Part C indicates the secondary structural element of proteins, where red denotes alpha helices and blue beta strands for 3NQS.

Molecular dynamics simulations

The Desmond-Schrodinger software was used to conduct the simulation studies. The RMSF of the atomic sites of ligand on 3NQS are shown in Figure 3, D. In the iNOS-MA complex, initial simulations indicate a protein conformation stability. Structured adjustment is marked by progressive RMSD rise. After 20 ns, it fluctuates but stabilizes, indicating protein equilibrium. The ligand's low RMSD early on signals stable binding. In certain simulation stages, significant oscillations may indicate ligand structural changes or insufficient binding affinity. High peaks indicate loop or surface-exposed residue flexibility (Figure 3, E). The RMSD analysis suggests protein stability but dynamic binding or ligand instability. Figure 3 (F) indicates that the MA interacts with numerous amino acid residues on 3NQS. The bar chart shows that the residue interactions ASP-382, GLU-377, and other highlighted residues have the highest interaction percentages, demonstrating their relevance to ligand binding (G).

PCA analysis

It is used to characterize the protein dynamics by examining the collective motions in MD simulation trajectories. The stability of the graph depicting the eigenvalues of proteins versus the eigen-vector index (MA-3NQS) was shown in Figure 3 (H). The alterations were systematically recorded and graphed across three principal components, namely PC1, PC2, and PC3. The clusters of MA-3NQS, PC1, accounted for 26.34% of the total variance. PC2 accounted for 14.17% of the overall variance. On the other hand, PC3 accounts for 7.57% of the total variance. PC3 is considered a more stable target-MA binding complex than PC1 and PC2 because of lower variability resulting from its compact structural nature. The observed motion shows biologically relevant flexibility rather than instability. The degree of flexibility is represented by blue, red color shows the least flexibility, while white indicates moderate movement.

MWM test

This test assesses memory deficits and cognitive decline in $AlCl_3$-induced neurodegenerative mice. In all groups, the escape latency declines over successive learning sessions. In this hidden-platform probe test, $AlCl_3$-prompted mice showed a high latency time compared with saline control,

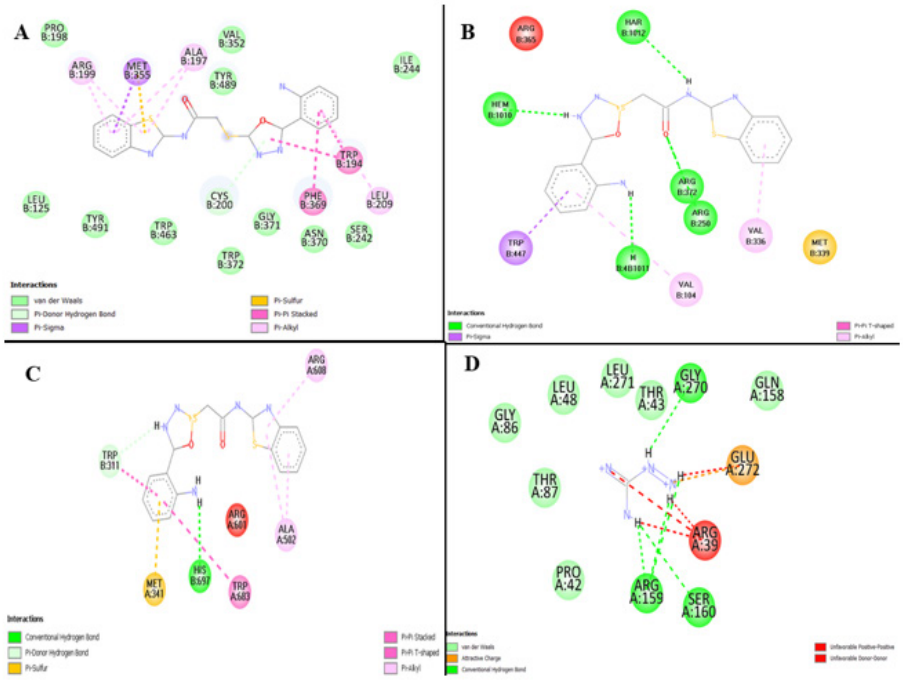

Figure 2. Examining the binding interactions of 2-{[5-(2-aminophenyl)-1,3,4-oxadiazol-2-yl] sulfanyl}-N-(1,3-benzothiazol-2-yl)acetamide (MA) with NOS protein isoforms
(A) iNOS, (B) nNOS, and (C) eNOS. The interactions were analyzed in silico, demonstrating binding affinities for different amino acid residues through the Discovery Studio client version 2021

mitigating memory deficit (Figure 4, $^{###}P<0.001$ vs saline group). The test analysis indicates that MA administration at the doses of 5, 10, and 20 mg/kg substantially improves latency time when compared to the $AlCl_3$ control group, as shown in A, and also ameliorates memory impairment ($^{**}P<0.01$, $^{***}P<0.001$ vs $AlCl_3$ group). During a four-day trial period, the animal's ability to memorize and learn the hidden platform location is evaluated. The test analysis revealed that $AlCl_3$ disease-control mice spent less time in the target quadrant than the control group ($^{###}P<0.001$ vs saline group). Upon MA (5, 10, and 20 mg/kg) treatment, the animals show significantly enhanced memory and spatial learning in a dose-dependent manner ($^{***}P<0.001$ vs $AlCl_3$). Additionally, B represents MA treatment with the inhibitor

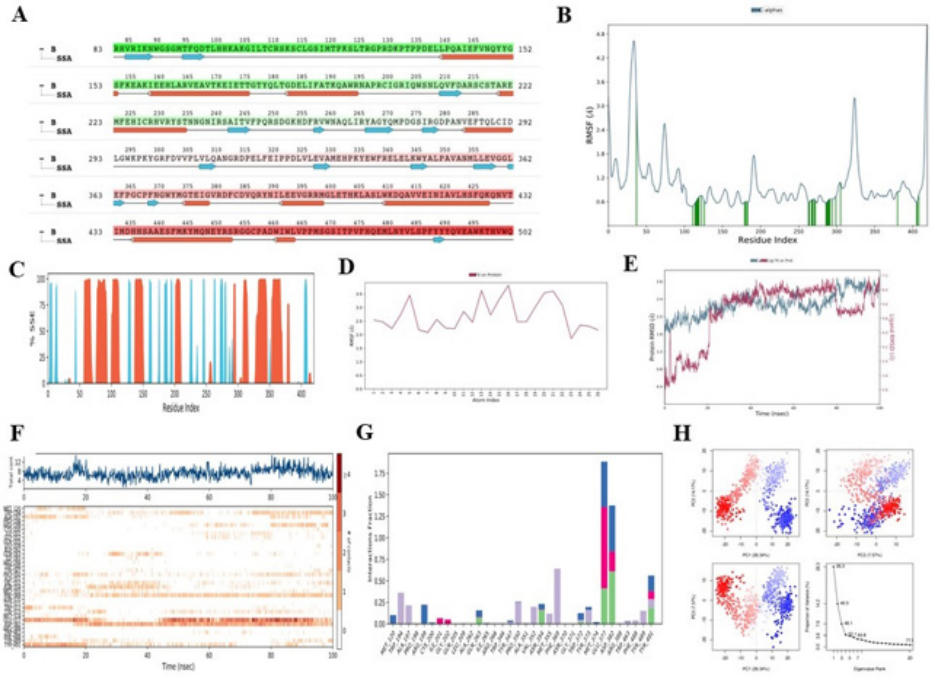

Figure 3. Describes the structural and dynamic characteristics of iNOS (3NQS) with 2-{[5-(2-aminophenyl)-1,3,4-oxadiazol-2-yl] sulfanyl}-N-(1,3-benzothiazol-2-yl)acetamide (MA)
A-C represents the basic protein's properties, D-E represents the RMSD and RMSF trajectory, (F) exhibits a time-based representation of the many contacts and interactions between MA and 3NQS, Key protein interactions between MA and 3NQS (G), PCA (PC1-PC3) summarizes the significant conformational changes (H).

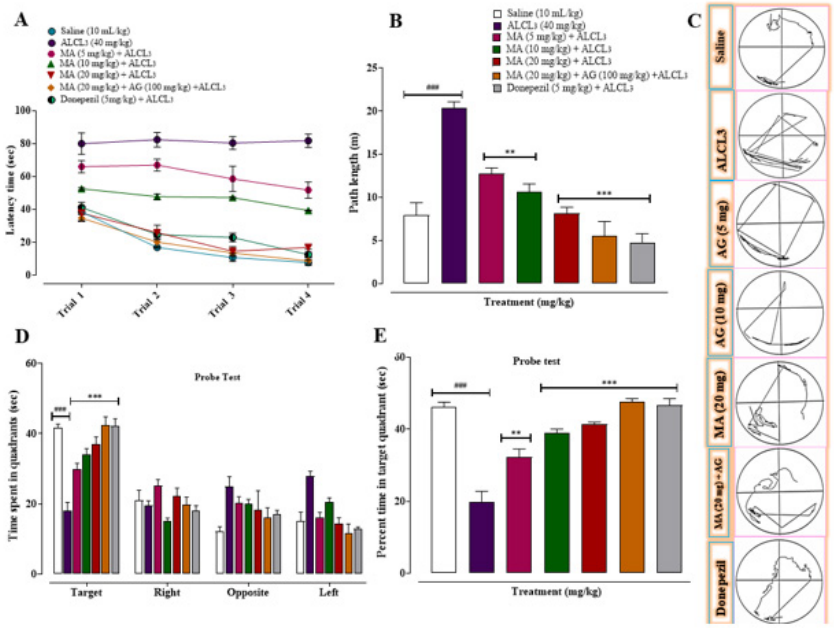

Figure 4. Represents the effects of 2-{[5-(2-aminophenyl)-1,3,4-oxadiazol-2-yl] sulfanyl}-N-(1,3- benzothiazol-2-yl)acetamide (MA), aminoguanidine (AG) and donepezil on average latency time (sec) of mice to find the probe from day 1 to 4 (A), Path length (m) B, Path tracings via ANY-maze (C), time spent (sec) in different quadrants (D), and percent time spent in target quadrant € during probe trial of mice in trial 1, 2, 3 and 4 in Morris water maze test Values expressed as mean ± SEM (n=6). One-way ANOVA with *post hoc* Tukey's test. ###P<0.001 vs saline group, **P<0.01, ***P<0.001 vs $AlCl_3$ group.

(5 mg/kg), which further improves memory function. C shows the % time spent in the target quadrants. Animals treated with MA spend more time in target quadrants than the $AlCl_3$-prompted neurodegenerative group (P<0.01, ***P<0.001 vs $AlCl_3$ group). D and E show the pathlength (m); the $AlCl_3$-induced disease group showed an increase in the path length. Administration of MA shortens the pathlength over successive training trials, showing improvement in learning and spatial memory. Administration of MA with AG further enhances the effect, highlighting the role of iNOS inhibition in the neuroprotective effect. Donepezil also improved the memory functioning.

EPM test

The EPM test was used to evaluate memory deterioration in mice (Figures 5A and 5B). $AlCl_3$ (40 mg/kg) induced animals significantly decreased the number of entries as well as time spent (###P<0.001 vs saline group) in the open arm. The treatment of animals with MA (5, 10 and 20 mg/kg) alone as well as with inhibitor (100 mg/kg) enhanced the number of entries and time spend in open arm showing an improvement in spatial memory deterioration induced by $AlCl_3$ (*P<0.05, **P<0.01, ***P<0.001vs $AlCl_3$ induced group). The standard drug (Donepezil) at a dose of 5 mg/kg increases the number of entries and time spent similarly (*P<0.05, **P<0.01, ***P<0.001, vs $AlCl_3$ group).

OFT

The anxiety-like behavior in the animal was assessed using OFT (Figure 5). In OFT, $AlCl_3$-induced disease control mice showed fewer entries in the central zone (C), along with reduced time spent in the center square (D), and also effects on the number of rearing (E) (###P<0.001 vs saline group). The administration of MA (5, 10 and 20 mg/kg) and MA (20 mg/kg) + AG (100 mg/kg) significantly increase time spent in the central zone along with the number of entries and number of rearing implicating the possible implication of iNOS in $AlCl_3$-induced neurodegeneration (*P<0.05, **P<0.01, ***P<0.001 vs $AlCl_3$ group). The standard drug Donepezil (5 mg/kg) similarly increases time spent in open arms (***P<0.001 vs $AlCl_3$ group).

Y-Maze test

The Y-maze test was used to analyze the memory alterations in mice (Figure 5, F and G). Compared with the saline-treated group, animals treated with $AlCl_3$ (40 mg/kg) showed significantly fewer entries (###P<0.001 vs saline group) and a lower % alternations. Treatment with MA at 5, 10, and 20 mg/kg increased the number of entries and % alternations, indicating an improvement in spatial memory deficits and cognitive impairment induced by $AlCl_3$ (*P<0.05, **P<0.01, ***P<0.001). The administration of MA (20 mg/kg) with AG (100 mg/kg) produces a further positive effect on memory restoration. The standard drug at a 5 mg/kg dose also reduces the number of entries and the % alterations in a manner similar to that of the $AlCl_3$ group (*P<0.05, **P<0.01, ***P<0.001).

Effect of different doses of MA on multiple time points

The dose-dependent effect of MA on escape latency (s) was assessed on different days to evaluate learning behavior and memory alterations in the MWM (Figure 6). A reduction in escape latency was observed throughout the study period (i.e., 29 days) in all MA-treated groups (Figure 1). In the saline-treated group, escape latencies on days 15 and 29 were 29.4 ± 3.1 and 16.8 ± 1.9 s, respectively. In the $AlCl_3$-induced disease group, the escape latency was increased continuously up to the 29th day (91.8 ± 5, ###P vs Saline group). The treatment of animal with MA at dose of 5, 10 and 20 mg/kg remarkable reduce the escape latency in dose dependent manner (42.8 ± 3.6, 36.4 ± 2.9, 33 ± 2.6 at day 15th and 33.8 ± 1.9, 24.4 ± 2.6, 27 ± 2.4 at day 29th) in comparison to $AlCl_3$ group (*P<0.05, **P<0.01, ***P<0.001). MA with AG (100 mg/kg) significantly decreased escape latency (day 15th: 27 ± 2.3; day 29th: 19.8 ± 2.7; ***P<0.001 vs

$AlCl_3$ group). The standard drug (donepezil, 5 mg/kg) also produces an effect on escape latency (day 15th: 24.4 ± 2.7; day 29th: 13.4 ± 2.2; ***P<0.001 vs $AlCl_3$ group).).

Effect on oxidative stress markers

$AlCl_3$-induced control mice significantly decreased GST, GSH, and catalase, along with the marked increase in LPO levels compared with the saline group (###P<0.001 vs saline group). Administration of MA at doses of 5, 10, and 20 mg/kg increases the anti-oxidant enzyme levels in the brain with variable degrees of expression (Table 2). The levels of GSH, Catalase, and GST in the compound-treated group were remarkably increased compared to those in the saline-treated group, whereas there was a marked decrease in the levels of LPO. The compound, when administered with the inhibitor, further enhances the pharmacological effect. The standard drug (donepezil, 5 mg/kg) increased GSH, GST, and catalase levels and decreased LPO levels (**P<0.01, ***P<0.001 vs $AlCl_3$-induced disease group).

Effect of MA on neuromodulatory cytokines involved in AD

The expression of cytokines such as IL-6, IL-1ß, IFN-γ, p-NFKB, TNF-α, *ptau*, and β-amyloid was prominently enhanced in the $AlCl_3$-disease control group when compared to saline control mice (###P<0.001). Administration of MA (20 mg/kg) and MA (20 mg/kg) with inhibitor (100 mg/kg), declines the expression of AD markers in brain tissue when compared with the $AlCl_3$ group (*P<0.05, **P<0.01, ***P<0.001). Moreover, the specific deficit of TGF-ß1 signaling was observed in the AD group; administration of MA, AG, and donepezil restores the neuroprotective role of TGF-β1 (Figure 7).

Effect of MA on complex I, complex IV, and ATP levels

The mitochondrial functioning by measuring Complex I, Complex IV, and ATP levels was evaluated in the brain tissue of the disease, and MA-treated animals (Figure 8).

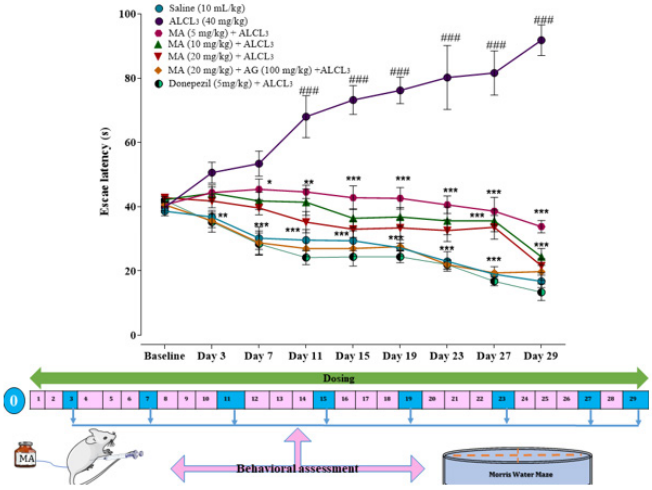

Figure 6. Represents the dose-dependent neuroprotective effect of MA on mice's escape latency at multiple time points in $AlCl_3$-induced Alzheimer's disease

Values are expressed as Mean ± SEM. Two-way analysis of variance with *post hoc* Tukey's test. ###P<0.001 vs saline group, *P<0.05, **P<0.01 and ***P<0.001 vs $AlCl_3$ induced group. MA: 2-{[5-(2-aminophenyl)-1,3,4-oxadiazol-2-yl] sulfanyl}-N-(1,3-benzothiazol-2-yl)acetamide; AG: aminoguanidine

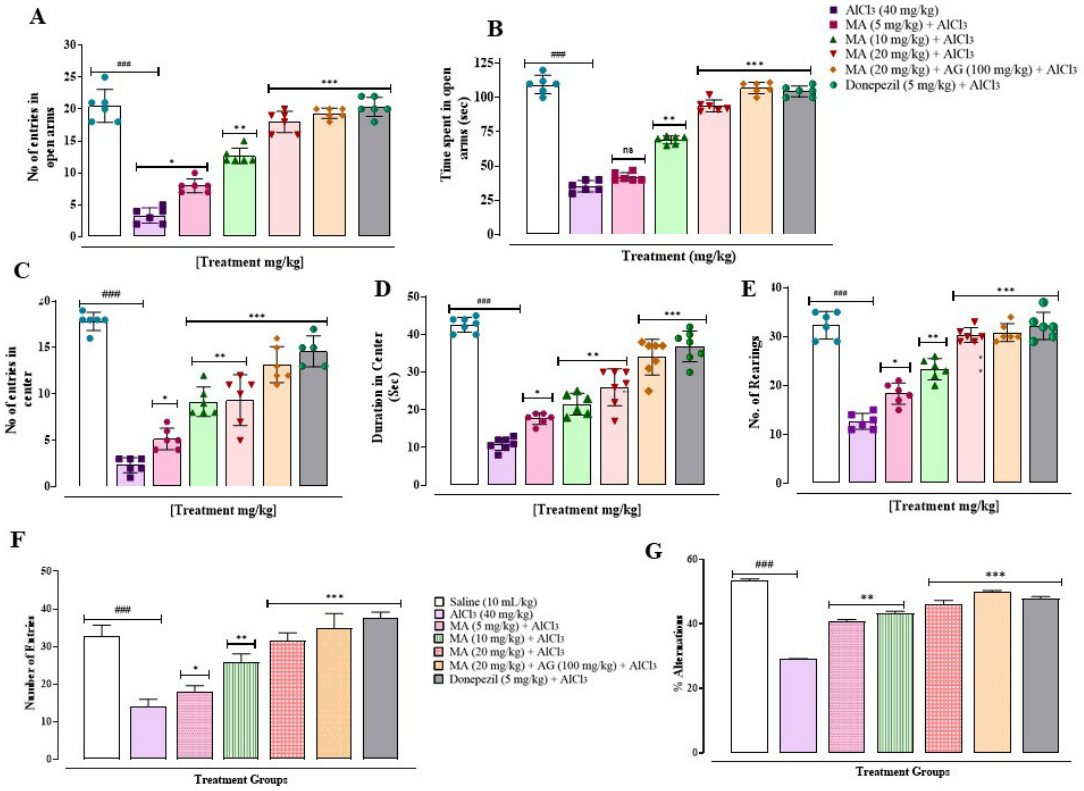

Figure 5. Represents the effects of 2-{[5-(2-aminophenyl)-1,3,4-oxadiazol-2-yl] sulfanyl}-N-(1,3-benzothiazol-2-yl)acetamide (MA), AG and donepezil on number of entries

(A) and time spent in open arm (sec) (B) of mice in Elevated plus maze test, number of entries in center (C), duration (sec) in center (D) and number of rearing (E) of mice in open field test. F and G represent the effect on the number of entries and % alternation of mice in the Y-maze test. Values are expressed as mean ± SEM (n=6). One-way analysis of variance with *post hoc* Tukey's test. ###P<0.001 vs saline group, *P<0.05, **P<0.01, and ***P<0.001 vs $AlCl_3$ group.

Table 2. Effect of MA, AG, and Donepezil on oxidative stress markers in mice

Treatment groups	GST (µM CDNB conjugate/min/mg protein)	GSH (µM/mg of protein)	Catalase (µM of H_2O_2/min/mg protein)	LPO (Tbars-nM/min/mg of protein)
Saline (10 ml/kg)	40.5± 0.29	56.25 ±0.577	50.417 ±0.44	44.417 ± 0.96
ALCL3 (40 mg/kg)	19.25 ±0.72###	22.67 ±1.24###	18.667 ±0.58###	148.67 ±0.88###
MA (20 mg/kg) + ALCL3 (40 mg/kg)	24.75 ±0.58**	36.5 ±0.52**	30.75 ±1.01**	106.6 ± 6**
MA (20 mg/kg) + AG (100 mg/kg) + ALCL3 (40 mg/kg)	33.25± 0.57***	45.667 ±1.16***	39.917 ±1.66**	91.67 ±1.2**
Donepezil (5 mg/kg) + ALCL3 (40 mg/kg)	37.08 ±0.65***	52.75 ±0.58***	44.58± 0.82**	81.33 ±1.86***

All data were analyzed by one-way ANOVA followed by *post hoc* multiple comparison test. Data were presented as the mean ± SEM. Symbol ∗shows a significant difference vs $AlCl_3$, and # shows a significant difference vs saline. GST: glutathione-S transferase; GSH: glutathione; LPO: Lipid peroxidase; MA: 2-{[5-(2-aminophenyl)-1,3,4-oxadiazol-2-yl] sulfanyl}-N-(1,3-benzothiazol-2-yl)acetamide; AG: aminoguanidine.

A significant decline in Complex I, Complex IV, and ATP levels was observed in the $AlCl_3$-induced disease group, indicating mitochondrial dysfunction, impaired oxidative phosphorylation, and reduced energy. Treatment of animals with MA and MA with AG restores the activity of Complex I and IV, as well as causes elevation of ATP levels compared with the $AlCl_3$ group (***P<0.001). The donepezil-treated group also showed restoration of enzyme activity as well as ATP levels (***P<0.001 vs $AlCl_3$ group).

Effect of MA on the expression of NO level in the mouse brain

NO expression was assessed in animal brains to estimate NO production using the Griess reagent method (Table 3). The levels of NO were found to be elevated in the $AlCl_3$-induced disease group compared to the saline group (### P<0.001), while the expression was reduced in the MA-treated group (*P<0.05 vs $AlCl_3$-induced disease group). The effect was further enhanced in combination with MA and AG (**P<0.01 vs $AlCl_3$-induced disease group). The positive control also shows a significant impact (***P<0.001 vs $AlCl_3$-induced disease group).

Histopathological examination

CV staining of brain tissues reveals significant neuronal alterations in the hippocampus and cortex in the $AlCl_3$-induced disease group compared with the Saline group (Figure 9). The saline-treated group revealed neuronal integrity with well-defined boundaries and prominent nuclei. The $AlCl_3$ (40 mg/kg) treated disease group showed degeneration of neuronal tissue with p, shrunken cells with irregular outline, and loss of neuronal density. Animals administered with MA (20 mg/kg) showed an improvement in neuronal morphology with better cellular architecture, demonstrating a neuroprotective effect. Treatment of animals with MA (20 mg/kg) +AG (100 mg/kg) depicts a more prominent effect on restoration of neuronal function, suggesting the synergistic effect of iNOS inhibition and restoration of nitrosative stress. Decreased vacuolization and neuronal integrity were also observed in the donepezil (5 mg/kg) treated group.

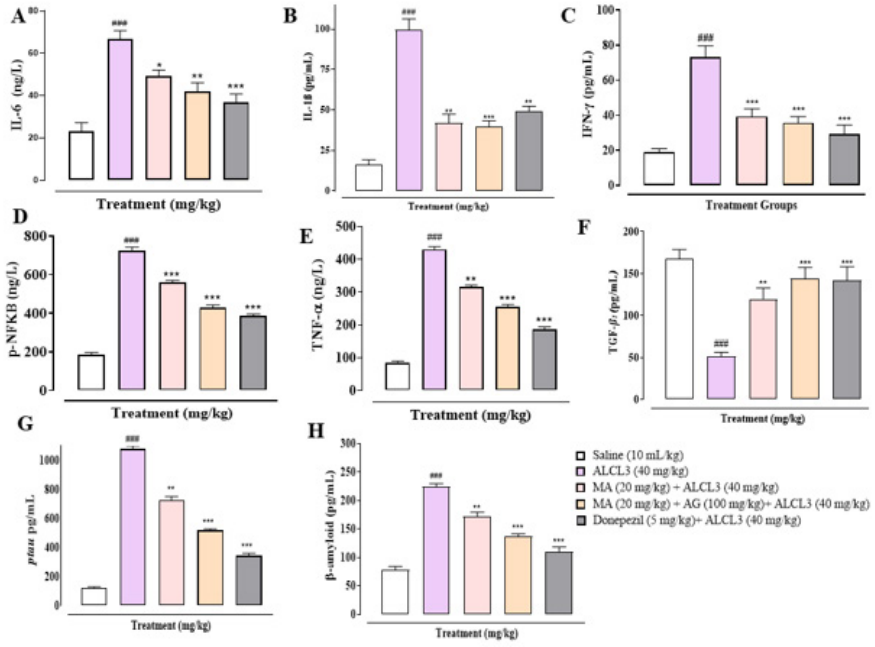

Figure 7. Effect of MA, AG, and donepezil on (A) Interleukin-6 IL-6, (B) Interleukin-1-beta IL-1ß, (C) Interferon gamma IFN-γ, (D) Nuclear factor kappa B p-NFKB, (E) Tumor necrosis Factor alpha TNF-α, (F) Tissue growth factor beta 1 TGF-β1, (G) phosphorylated tau ptau, and (H) beta amayloid (β-amyloid) expression in $AlCl_3$-treated mice brain tissues, measured by enzyme-linked immunosorbent assay (ELISA) technique

Data expressed as mean ± SEM (n=3). One-way ANOVA with *post hoc* Tukey's test. ###P<0.001 vs saline group, *P<0.05, **P<0.01, ***P<0.001 vs $AlCl_3$ group. MA: 2-{[5-(2-aminophenyl)-1,3,4-oxadiazol-2-yl] sulfanyl}-N-(1,3-benzothiazol-2-yl)acetamide; AG: aminoguanidine.

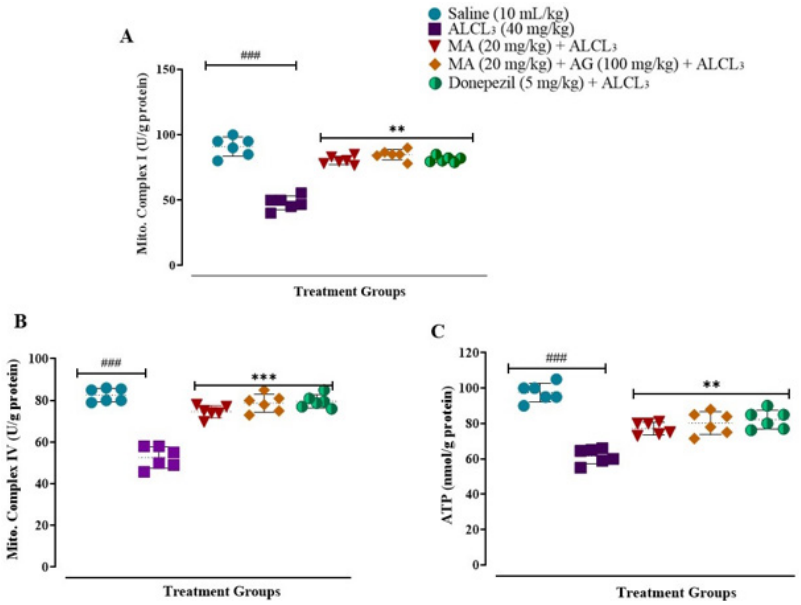

Figure 8. Effect of MA, AG, and donepezil on Complex I (A), Complex IV (B), and ATP (C) levels in the $AlCl_3$-induced mouse model of Alzheimer's
Values are expressed as mean± SEM. One-way ANOVA with *post hoc* Tukey's test was used. ### P<0.001 vs saline, *P<0.05, **P<0.01 and ***P<0.001 vs $AlCl_3$. MA: 2-{[5-(2-aminophenyl)-1,3,4-oxadiazol-2-yl] sulfanyl}-N-(1,3-benzothiazol-2-yl)acetamide; AG: aminoguanidine.

mRNA expression profiling by RT-PCR

To assess the potential involvement of the iNOS pathway in AD, we measured iNOS protein expression in the $AlCl_3$-augmented disease group and the compound-treated groups. iNOS expression was high in the $AlCl_3$-treated disease group (###P<0.001 vs saline group). Treatment with MA (20 mg/kg) alone or with the inhibitor (100 mg/kg) decreased expression compared with the $AlCl_3$-induced disease group (Figure 10). The standard drug (donepezil, 5 mg/kg) also shows similar results (*P<0.05, **P<0.01, ***P<0.001 vs $AlCl_3$ group).

Western blot analysis

Western blot analysis of brain tissues revealed increased iNOS levels in the $AlCl_3$-induced disease group. The treatment of animals with MA (20 mg/kg), MA (20 mg/kg) with iNOS inhibitor, AG (100 mg/kg), and donepezil (5 mg/kg) showed a relative decrease in expression levels compared to the saline (10 ml/kg) treated group (Figure 11).

Discussion

The neuro-restorative attribute of oxadiazole-benzothiazole hybrid (MA) in $AlCl_3$-prompted AD mice was mediated through modulation of nitrosative and oxidative stress, inflammatory cytokines, and decreased protein expression of iNOS. Our study demonstrated that administering MA to mice substantially improved memory and learning, as indicated by behavioral analyses in the Y-Maze, MWM, EPM, and OFT. Furthermore, pronounced alterations were observed in the concentrations of GSH, GST, catalase, and LPO, indicating the involvement of oxidative stress in neurodegeneration. Additionally, MA treatment led to down-regulation of inflammatory markers such as IL-6, IL-1β, IFN-γ, p-NF-κB, TNF-α, TGF-β1, *ptau*, and β-amyloid, which are linked to various cellular mechanisms. The administration of MA also causes notable improvements in the NO levels, provoked by the consumption of $AlCl_3$. Molecular docking is a key tool in drug discovery and development. *In silico* analysis determines the affinity of a ligand molecule towards the targeted protein. This technique not only suggests target selectivity but also enables the researcher to evaluate the compound associated with it (39). In continuity with our proposed mechanism, MA was docked with target proteins NOS isoforms involved in the pathophysiology of AD. The docking score indicates the high binding affinity with iNOS (PDB ID: 3NQS), and further, the simulation results showed a stable interaction as demonstrated by its RMSF and RMSD values. The lower the

Table 3. Effect of MA on NO expression in the mouse brain

Sr.no.	Groups	NO (µmol/mg of protein)
1	Saline (10 ml/kg)	40.15 ± 1.28
2	$AlCl_3$ (40 mg/kg)	102.13 ± 1.8###
3	MA (20 mg/kg) + $AlCl_3$ (40 mg/kg)	88.52 ± 1.33*
4	MA (20 mg/kg) + AG (100 mg/kg) + $AlCl_3$ (40 mg/kg)	72.85 ± 1.42**
5	Donepezil (5 mg/kg) + $AlCl_3$ (40 mg/kg)	61.62 ± 1.1***

Values were expressed as Mean± SEM (n = 3). One-way ANOVA followed by *post hoc* Tukey's test. P<0.001 vs Saline *P<0.05, **P<0.01 and ***P<0.001 vs $AlCl_3$.
MA: 2-{[5-(2-aminophenyl)-1,3,4-oxadiazol-2-yl] sulfanyl}-N-(1,3-benzothiazol-2-yl)acetamide

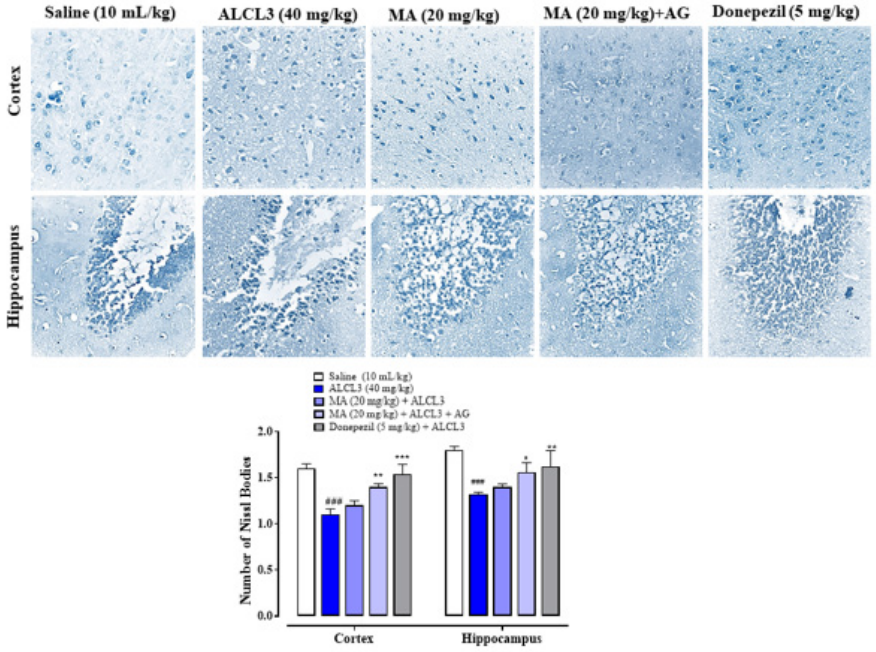

Figure 9. Histopathological slides showing the effect of MA, MA+AG, and donepezil in $AlCl_3$-induced Alzheimer 's-like disease in mice using the cresyl violet Nissl staining technique

Bar 50 µm, magnification 40X. MA: 2-{[5-(2-aminophenyl)-1,3,4-oxadiazol-2-yl] sulfanyl}-N-(1,3-benzothiazol-2-yl)acetamide; AG: aminoguanidine.

variation in the RMSD, the stronger the interaction of the ligand with the target (40). Based on these *in silico* analyses, MA was further evaluated for its therapeutic efficacy in animal models. Metals such as Aluminum have been widely recognized as risk factors for neurodegeneration, mediating neuronal alterations via oxidative stress (41). The previous literature highlighted the link between $AlCl_3$ administration and the development of neurological disease, including AD. $AlCl_3$ is widely used in the chemical industry for the production of paints, lubricants, rubber, antiperspirants, preservatives, insecticides, and medicines. $AlCl_3$ exhibits deleterious properties and can cause toxic effects through consumption of contaminated drinking water and food (42). Al is a well-established neurotoxic substance capable of producing neurodegeneration and

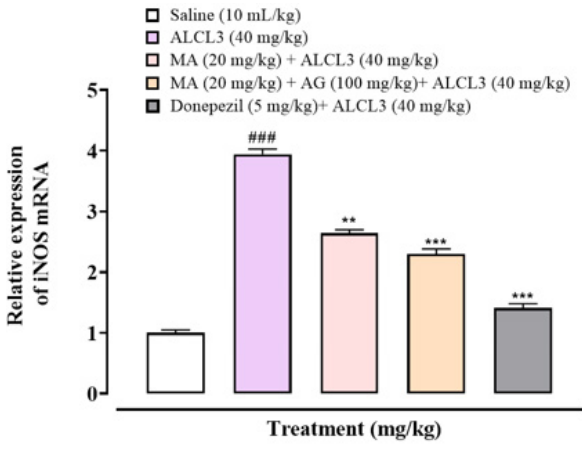

Figure 10. Graphical representation indicating the effect of MA, AG, and Donepezil on mRNA expression of iNOS in $AlCl_3$-induced neurodegeneration in mice, using the real time-polymerase chain reaction (RT-PCR) technique

Data expressed as mean ± SEM (n = 3). One-way ANOVA with *post hoc* Tukey's test. ###P<0.001 vs saline group, **P<0.01, ***P<0.001 vs $AlCl_3$ group. MA: 2-{[5-(2-aminophenyl)-1,3,4-oxadiazol-2-yl] sulfanyl}-N-(1,3-benzothiazol-2-yl)acetamide; AG: aminoguanidine.

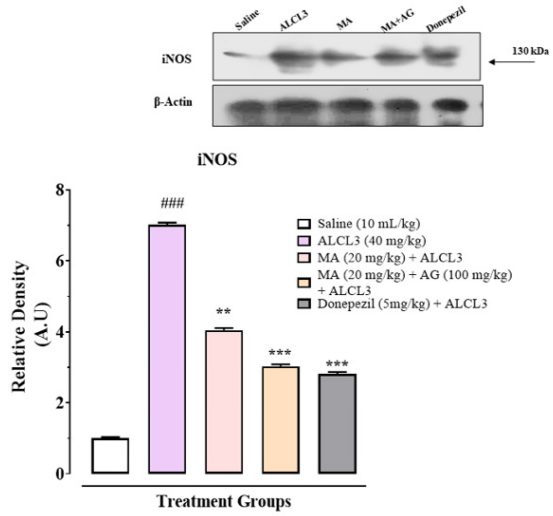

Figure 11. Inhibitory effect of MA, MA+AG, and Donepezil against iNOS and β-actin expression in $AlCl_3$-induced neurodegeneration in mice using the Wstern blot technique

Data expressed as Mean ±SEM (n=3). One-way ANOVA with *post hoc* Tukey's test. ###P<0.001 vs saline group, **P<0.01, *** P<0.001 vs $AlCl_3$ group. MA: 2-{[5-(2-aminophenyl)-1,3,4-oxadiazol-2-yl] sulfanyl}-N-(1,3-benzothiazol-2-yl) acetamide; AG: aminoguanidine.

causing symptoms similar to those of AD. The probable mechanisms underlying neurotoxicity include the augmentation of oxidative stress, neuroinflammation (9), enhanced Aβ accumulation, increased tau phosphorylation, and apoptosis (43). When compared to the saline control group, $AlCl_3$-induced mice showed a progressive increase in the escape latency time, reflecting cognitive decline such as memory impairment and decreased learning ability. The outcome of our study is consistent with previous studies on $AlCl_3$-induced AD in animals (44-46). The current study elaborated that the treatment of mice with MA alone and with an iNOS inhibitor produces a significant reduction

in escape latency. In addition, animals in the treatment group spent more time in the target quadrant during the probe test, revealing an improvement in memory retention. In the EPM test, MA-treated animals show a greater number of entries and spend more time in the open arm as compared to the disease control, indicating the neuroprotective potential of MA in AD**.** In the Y-maze test, mice showed increased number of entries and % alternation in compound-treated groups, indicating restoration of memory function. In OFT, MA-treated mice show a greater number of entries and spend more time in the center as compared to the $AlCl_3$-induced disease group, indicating the curative potential of MA in neurodegeneration.ROS-mediated damage plays a pivotal role in the development and emergence of AD owing to its potential effect on Aβ and tau protein accumulation, mitochondrial dysfunction, and depletion of anti-oxidant enzymes such as catalase, GST, and GSH (47). The administration of $AlCl_3$ causes a substantial increase in oxidative stress markers (48), hence triggering the Aβ production and accumulation within the mouse brain, consequently leading to the manifestation of AD. The development of oxidative stress in the $AlCl_3$ disease control group was demonstrated by the increased levels of LPO along with decreased levels of GST, GSH, and catalase. These findings are consistent with the previous research demonstrated by Anynwu (49). Based on our investigation, it is conceivable to suggest that the administration of MA has the potential to modify the levels of oxidative stressors. The results of this investigation indicate that the administration of MA causes a considerable increase in the GST, GSH, and catalase activities while concurrently down-regulating the LPO levels. $AlCl_3$ exposure resulted in mitochondrial dysfunction, which is consistent with previous findings. Mitochondrial alteration leads to inhibition of complex I -IV and a decrease in ATP levels, causing loss of neuronal energy and synaptic dysfunction, characteristic symptoms of Alzheimer's. The treatment of animals with MA improves the functioning, depicting the anti-oxidative role of the compound in neuroinflammation. Administration of AG further enhances the effect, showing the involvement of iNOS suppression in improving mitochondrial functioning. The results from our study showed the neuroprotective role of MA in AD-like pathology.

Emerging evidence indicated the involvement of neuroinflammation as the earlier pathological event in the development of AD, even before the hallmark symptoms such as Aβ accumulation or tau hyperphosphorylation (50). A transcription factor called NFKB plays a fundamental role in the up-regulation of multiple genes relevant to inflammation. The neuronal damage in AD causes NFKB to be stimulated in different regions of the brain (51). During neuroinflammation, the nuclear localization of NFKB is produced through the phosphorylation of factor IκBα. The TGF-β1 signaling was declined in the AD brain, causing neuronal toxicity, Aβ accumulation, and neurodegeneration. Moreover, TGF-β1 impairment also contributes to tau pathology. Recent studies have demonstrated the neuroprotective role of TGF-β1 in various models of AD (52, 53). Drugs increasing the TGF-β1 level in the brain cause beneficial neuro-modulatory effects. The up-regulated level of TGF-β1 was demonstrated in the MA and AG treated groups, which is aligned with previous findings. There is a down-regulation of TGF-β1 level in the $AlCl_3$-induced disease group. The phosphorylation and beta-amyloid accumulation consequently augment the activation of proinflammatory cytokines such as TNF-α, IL-6, IL-1β, IFN-γ, and iNOS, leading to the initiation of an inflammatory response (42). Our results suggested that MA administration exerts a significant inhibitory effect on the $AlCl_3$-induced elevated levels of IL-6, IL-1β, TNF-α, IFN-γ, iNOS, and NFKB, recognized as potential inflammatory indicators.

Based on the previous research, iNOS is known to be the major contributor among the three isoforms in the progression of neurodegenerative disorders such as AD. Previous findings suggested that iNOS and ultimately NO production are involved in various mechanisms leading to the development of neurodegeneration (54). During neuroinflammation, production of NO by iNOS is up-regulated and is considered a major determinant of oxidative stress-associated neurodegeneration (10). The administration of $AlCl_3$ resulted in increased NO expression, consistent with prior research that indicated its increased expression in the animal model of AD induced by aluminum (37). The decrease in NO expression by the treated group suggests a novel option for the management of AD. The effect was further added by the aminoguanidine, suggesting a more beneficial effect in combination. Currently, no complete curative treatment for AD is available; rather, the limited drug options available to clinicians provide only symptomatic relief (55). The current study's findings demonstrated that MA alone or in combination with AG can strongly prevent $AlCl_3$-induced alteration in the iNOS level, as indicated by the mRNA expression and western blot analysis. Based on this evidence, MA may ameliorate $AlCl_3$-provoked cognitive decline via modulation of oxidative stress, cytokines, and iNOS inhibition.

Conclusion

To conclude, the current study validates that MA could serve as a multi-site acting compound for the management of AD. MA demonstrated substantial neuroprotective effects in $AlCl_3$-induced neuronal alteration, with notable improvements in behavioral alteration, such as cognitive deficit and memory loss. Furthermore, MA significantly down-regulated inflammatory cytokines such as IL-6, IL-1ß, IFN-γ, NFKB, TNF-α, β-amyloid, and p-*tau*. MA also ameliorated oxidative stress and mitochondrial dysfunction induced by $AlCl_3$. The RT-PCR expression and western blot analysis show a reduction in iNOS mRNA level, while ELISA assays also confirmed decreased levels of β-amyloid and *p-tau* proteins. Notably, our results exhibited the involvement of the iNOS pathway in the aforementioned neuromodulatory effect of MA, suggesting it to be a potential therapeutic candidate for the management of AD (Figure 12).

Acknowledgment

The results presented in this paper were part of a student's thesis.

Ethical Approval

This study was performed in accordance with ARRIVE guidelines. Prior approval was obtained from the Research Ethical Committee (REC) at Riphah Institute of Pharmaceutical Sciences, Pakistan (reference no. REC-RIPS-2022/15). After anesthetizing mice with a mixture of xylazine (9 mg/kg) and ketamine (90 mg/kg) intraperitoneally, mice were decapitated. All efforts were made to minimize animal suffering.

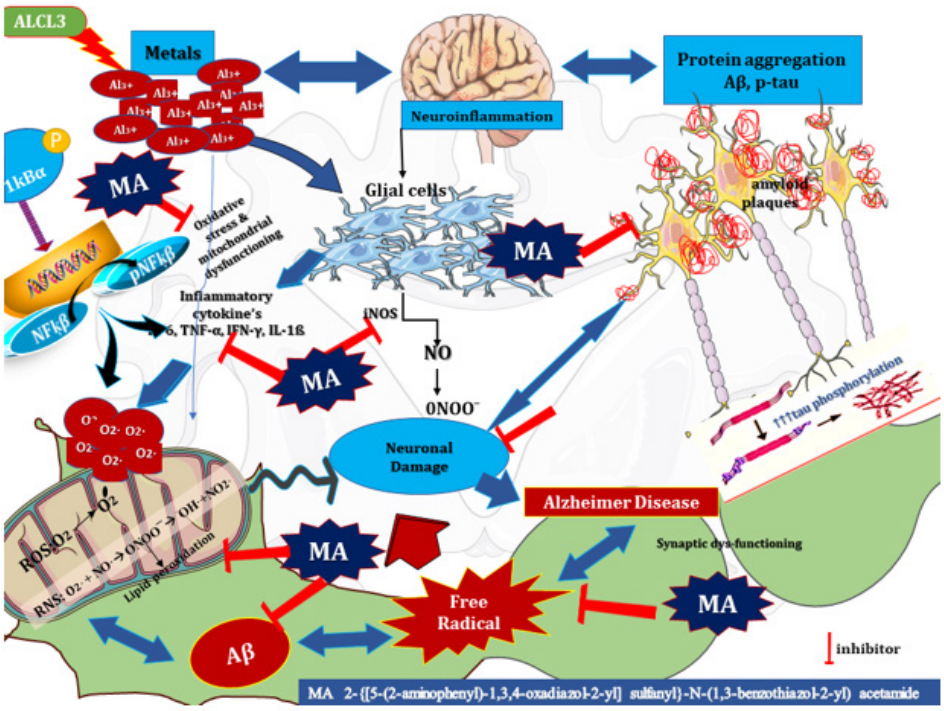

Figure 12. Illustration of possible mechanisms underlying the potential neuroprotective effect of MA and possible involvement of iNOS against $AlCl_3$-induced neurodegeneration
MA: 2-{[5-(2-aminophenyl)-1,3,4-oxadiazol-2-yl] sulfanyl}-N-(1,3-benzothiazol-2-yl)acetamide; AG: aminoguanidine

Data Availability

Data is available on request from the corresponding author.

Financial Declaration

This research project did not receive any specific grant from funding agencies in the public, commercial, or not-for-profit sectors.

Authors' Contributions

AU K conceptualized the study and developed the methodology. AM M conducted experiments, formal analyses, and investigations. AM M and N GQ worked on writing the original draft. F A performed MD simulations. H N, AM M, and N GQ contributed to the review and editing of the manuscript. AU K supervised the project. All authors approve this final version of the manuscript for publication.

Conflicts of Interest

The authors declare no conflicts of interest.

Declaration

We have not used any AI tools or technologies to prepare this manuscript.

References

1. Botto R, Callai N, Cermelli A, Causarano L, Rainero I. Anxiety and depression in Alzheimer's disease: A systematic review of pathogenetic mechanisms and relation to cognitive decline. J Neurol Sci 2022; 43:4107-4124.
2. Gyimesi M, Okolicsanyi R, Haupt L. Beyond amyloid and tau: Rethinking Alzheimer's disease through less explored avenues. Open Biol 2024; 14:240035.
3. Sharma C, Kim SR. Oxidative stress: culprit or consequence in Alzheimer's amyloidopathy. Neural Regen Res 2023; 18:1948-1949.
4. Roy RG, Mandal PK, Maroon JC. Oxidative stress occurs prior to amyloid Aβ plaque formation and tau phosphorylation in Alzheimer's disease: Role of glutathione and metal ions. ACS Chem Neurosci 2023; 14:2944-2954.
5. Lushchak VI, Lushchak O. Interplay between reactive oxygen and nitrogen species in living organisms. Chem Biol Interact 2021; 349:109680.
6. Asiimwe N, Yeo SG, Kim M-S, Jung J, Jeong NY. Nitric oxide: Exploring the contextual link with Alzheimer's disease. Oxid Med Cell Longev 2016; 2016:7205747.
7. Justo AFO, Suemoto CK. The modulation of neuroinflammation by inducible nitric oxide synthase. J Cell Commun Signal 2022; 16:155-158.
8. Iova OM, Marin GE, Lazar I, Stanescu I, Dogaru G, Nicula CA, *et al.* Nitric oxide/nitric oxide synthase system in the pathogenesis of neurodegenerative disorders—an overview. Antioxidants 2023; 12:753.
9. Rahman A, Banu Z. Impact of Aluminium Chloride ($AlCl_3$) on Brain Function: A Review of Neurotoxic Mechanisms and Implications for Alzheimer's Disease. Trends Pharmacol Sci 2024; 10:355-366.
10. Stevanović I, Jovanović M, Čolić M, Jelenković A, Mihajlović R, Stojanović I, *et al.* The effect of aminoguanidine, an inducible nitric oxide synthase inhibitor, on AlCl3 toxicity in the rat hippocampus. Arch Biol Sci 2010; 62:981-991.
11. Martínez-Coria H, Arrieta-Cruz I, Gutiérrez-Juárez R, López- Valdés HE. Anti-inflammatory effects of flavonoids in common neurological disorders associated with aging. Int J Mol Sci 2023; 24:4297.
12. Ahmed SM, Tugcu G, Akkoc MK. The promising role of iNOS inhibitors in Alzheimers disease. J Fac Pharm Ankara 2024; 48:289-299.
13. Yadav KP, Rahman MA, Nishad S, Maurya SK, Anas M, Mujahid M. Synthesis and biological activities of benzothiazole derivatives: A review. Intell Pharm 2023; 1:122-132.
14. Yajing M, Sufang L, Qingfeng Z, Zhonghua L, Bin Y. Approved drugs and natural products at clinical stages for treating Alzheimer's disease. Chin J Nat Med 2024; 22:699-710.
15. Chowdhury R, Bhuia S, Rakib AI, Al Hasan S, Shill MC,

El-Nashar HA, *et al.* Gigantol, a promising natural drug for inflammation: A literature review and computational based study. *Nat Prod Res* 2024:1-17.
16. Bhuia MS, Islam T, Rokonuzzman M, Shamsh Prottay AA, Akter F, Hossain MI, *et al.* Modulatory effects of phytol on the antiemetic property of domperidone, possibly through the D2 receptor interaction pathway: *In vivo* and *in silico* studies. Biotech 2023; 13:116.
17. Islam MT, Chowdhury R, Al Hasan MS, Sheikh S, Bhuia MS, Bithi SA, *et al.* Possible hemoglobin enhancing effect of phytol in methotrexate-induced folate deficient Swiss albino mice: *In vivo* and *in silico* studies. Pharm Sci Adv 2024; 2:1-9.
18. Chowdhury R, Bhuia MS, Rakib AI, Hasan R, Coutinho HDM, Araújo IM, *et al.* Assessment of quercetin antiemetic properties: In vivo and in silico investigations on receptor binding affinity and synergistic effects. Plants 2023; 12:4189.
19. Madriwala B, Suma B, Jays J. Molecular docking study of hentriacontane for anticancer and antitubercular activity. Int J Chem Res 2022; 6:1- 4.
20. Guo Z, Mohanty U, Noehre J, Sawyer TK, Sherman W, Krilov GJCb, *et al.* Probing the α-helical structural stability of stapled p53 peptides: molecular dynamics simulations and analysis. Chem Biol Drug Des 2010; 75:348-359.
21. Phillips JC, Hardy DJ, Maia JD, Stone JE, Ribeiro JV, Bernardi RC, *et al.* Scalable molecular dynamics on CPU and GPU architectures with NAMD. J Chem Phys 2020; 153: 044130.
22. Lu C, Wu C, Ghoreishi D, Chen W, Wang L, Damm W, *et al.* OPLS4: Improving force field accuracy on challenging regimes of chemical space. J Chem Theory Comput 2021; 17:4291-4300.
23. Zayed AOH, Altarabeen M, AlShamaileh E, Zain SM. The potential of some functional group compounds substituted 8-Manzamine A as RSK1 inhibitors: molecular docking and molecular dynamics simulations. J Biomol Struct Dyn 2025:43:8347-8356.
24. Grant BJ, Skjaerven L, Yao XQ. The Bio3D packages for structural bioinformatics. Protein Sci 2021; 30:20-30.
25. Palma J, Pierdominici-Sottile G. On the uses of PCA to characterise molecular dynamics simulations of biological macromolecules: basics and tips for an effective use. ChemPhysChem 2023; 24:1-14.
26. Abdulmalek S, Suliman M, Omer O. Possible neuroprotective role of pomegranate juice in aluminum chloride induced Alzheimer's like disease in mice. J Alzheimers Dis Parkinsonism 2015; 5:2161-0460.
27. Ali T, Badshah H, Kim TH, Kim MO. Melatonin attenuates galactose-induced memory impairment, neuroinflammation and neurodegeneration via RAGE/NF-KB/JNK signaling pathway in aging mouse model. J Pineal Res 2015; 58:71-85.
28. Qazi NG, Malik AS, Alvi AM, Ali F, Badshah I, Nadeem H, *et al.* Regulating the NMDA/NR2B signaling pathway mediates anticonvulsant, antineuroinflammation, and anti-oxidative stress effects of 1, 3, benzothiazole derivative 1M in pentylenetetrazole-induced kindling in mice. Naunyn-Schmiedeberg's Arch Pharmacol 2025; 398:4037-4051.
29. Yoon SH, Kim B-H, Ye S-K, Kim M-H. Chronic non-social stress affects depressive behaviors but not anxiety in mice. Korean J Physiol Pharmacol 2014; 18:263-268.
30. Vorhees CV, Williams MT. Morris water maze: procedures for assessing spatial and related forms of learning and memory. Nat Protoc 2006; 1:848-858.
31. Razzaq S, Minhas AM, Qazi NG, Nadeem H, Khan A-u, Ali F, *et al.* Novel isoxazole derivative attenuates ethanol-induced gastric mucosal injury through inhibition of H+/K+-ATPase pump, oxidative stress and inflammatory pathways. Molecules 2022; 27:5065.
32. Seemab K, Khan A-u, Khan MI, Qazi NG, Minhas AM, Ali F. Anti-pruritic effect of L-carnitine against chloroquine-induced pruritus mediated via nitric oxide pathway. BMC Pharmacol Toxicol 2024; 25:32.
33. Faheem M, Ali SH, Khan AW, Alam M, Ilyas U, Zahoor M, *et al.* 1, 3, 4-Oxadiazole derivative attenuates chronic constriction injury induced neuropathic pain: a computational, behavioral, and molecular approach. Brain Sci 2020; 10:731.
34. Connolly NM, Theurey P, Adam-Vizi V, Bazan NG, Bernardi P, Bolaños JP, *et al.* Guidelines on experimental methods to assess mitochondrial dysfunction in cellular models of neurodegenerative diseases. Cell Death Differ 2018; 25:542-572.
35. Imran M, Al Kury LT, Nadeem H, Shah FA, Abbas M, Naz S, *et al.* Benzimidazole containing acetamide derivatives attenuate neuroinflammation and oxidative stress in ethanol-induced neurodegeneration. Biomolecules 2020; 10:108.
36. Piavchenko G, Soldatov V, Venediktov A, Kartashkina N, Novikova N, Gorbunova M, *et al.* A combined use of silver pretreatment and impregnation with consequent Nissl staining for cortex and striatum architectonics study. Front Neuroanat 2022; 16:940993.
37. Streyczek J, Apweiler M, Sun L, Fiebich BL. Turmeric extract(*Curcuma longa*) mediates anti-oxidative effects by reduction of nitric oxide, iNOS protein-, and mRNA-synthesis in BV2 microglial cells. Molecules 2022; 27:784.
38. Islam MA, Atanu MSH, Siraj MA, Acharyya RN, Ahmed KS, Dev S, *et al.* Supplementation of syringic acid-rich Phrynium pubinerve leaves imparts protection against allergic inflammatory responses by downregulating iNOS, COX-2, and NF-κB expressions. Heliyon 2023; 9:e13343.
39. Baskaran KP, Arumugam A, Kandasamy R, Alagarsamy S. *In silico* method for prediction of maximum binding affinity and ligand-protein interaction studies on Alzheimer's disease. Int J Res Granthaalayah 2020; 8:362-370.
40. da Fonseca AM, Caluaco BJ, Madureira JMC, Cabongo SQ, Gaieta EM, Djata F, *et al.* Screening of potential inhibitors targeting the main protease structure of SARS-CoV-2 via molecular docking, and approach with molecular dynamics, RMSD, RMSF, H-bond, SASA and MMGBSA. Mol Biotechnol 2024; 66:1919-1933.
41. Dey M, Singh RK. Neurotoxic effects of aluminium exposure as a potential risk factor for Alzheimer's disease. Pharmacol Rep 2022; 74:439-450.
42. Kazmi I, Afzal M, Imam F, Alzarea SI, Patil S, Mhaiskar A, *et al.* Barbaloin's chemical intervention in aluminum chloride induced cognitive deficits and changes in rats through modulation of oxidative stress, cytokines, and BDNF Expression. ACS Omega 2024; 9:6976-6985.
43. Raj K, Gupta G, Singh S. Spermine protects aluminium chloride and iron-induced neurotoxicity in rat model of Alzheimer's disease via attenuation of tau phosphorylation, amyloid-β (1–42) and NF-κB pathway. Inflammopharmacology 2021; 29:1777-1793.
44. Chernyuk D, Bol'shakova A, Vlasova O, Bezprozvanny I. Possibilities and prospects of the behavioral test "morris water maze". J Evol Biochem Physiol 2021; 57:289-303.
45. Kazmi I, Al-Abbasi FA, Afzal M, Nadeem MS, Altayb HN. Sterubin protects against chemically-induced Alzheimer's disease by reducing biomarkers of inflammation-IL-6/IL-β/TNF-α and oxidative stress-SOD/MDA in rats. Saudi J Biol Sci 2023; 30:103560.
46. Moftah HK, Mousa MH, Elrazaz EZ, Kamel AS, Lasheen DS, Georgey HH. Novel quinazolinone derivatives: Design, synthesis and in vivo evaluation as potential agents targeting Alzheimer disease. Bioorg Chem 2024; 143:107065.
47. Houldsworth A. Role of oxidative stress in neurodegenerative disorders: A review of reactive oxygen species and prevention by antioxidants. Brain Communications 2024; 6:1-12.
48. Wei Y, Liu D, Zheng Y, Li H, Hao C, Ouyang W. Protective effects of kinetin against aluminum chloride and D-galactose induced cognitive impairment and oxidative damage in mouse. Brain Res Bull 2017; 134:262-272.
49. Anyanwu E, Nwachukwu J, Obasi K, Ekwueme P, Anyanwu C. Fisetin attenuates $AlCl_3$-induced neurodegeneration by modulating oxidative stress and inflammatory cytokine release in adult albino wistar rats. Toxicol Rep 2024; 13:101812.
50. Garbuz D, Zatsepina O, Evgen'ev M. Beta amyloid, tau

protein, and neuroinflammation: an attempt to integrate different hypotheses of Alzheimer's disease pathogenesis. Mol Biol 2021; 55:670-682.
51. Babkina I, Sergeeva S, Gorbacheva L. The role of NF-κB in neuroinflammation. Neurochemical J 2021; 15:114-128.
52. Tiong SQ, Mohgan RN, Quek JY, Liew JYS, Wong GYS, Thang ZQ, *et al.* Inhibition of the transforming growth factor-β signaling pathway confers neuroprotective effects on beta- amyloid induced direct neurotoxicity and microglia mediated neuroinflammation. Neurol Res Int 2025; 2025: 1-13.
53. Yang C, Xu P. The role of transforming growth factor β1/ Smad pathway in Alzheimer's disease inflammation pathology. Mol Biol Rep 2023; 50:777-788.
54. Tewari D, Sah AN, Bawari S, Nabavi SF, Dehpour AR, Shirooie S, *et al.* Role of nitric oxide in neurodegeneration: function, regulation, and inhibition. Curr Neuropharmacol 2021; 19:114-126.
55. Srivastava S, Ahmad R, Khare SK. Alzheimer's disease and its treatment by different approaches: A review. Eur J Med Chem 2021; 216:113320.